 CMES, vol.12, no.3, pp.229-241, 2006

Buckling of Honeycomb Sandwiches: Periodic Finite Element Considerations

D. H. Pahr[1] **and F.G. Rammerstorfer**[1]

Abstract: Sandwich structures are efficient lightweight materials. Due to there design they exhibit very special failure modes such as global buckling, shear crimping, facesheet wrinkling, facesheet dimpling, and face/core yielding. The core of the sandwich is usually made of foams or cellular materials, e.g., honeycombs. Especially in the case of honeycomb cores the correlation between analytical buckling predictions and experiments might be poor (Ley, Lin, and Uy (1999)). The reason for this lies in the fact that analytical formulae typically assume a homogeneous core (continuous support of the facesheets). This work highlights problems of honeycomb core sandwiches in a parameter regime, where the transition between continuous and discrete support of the facesheets is studied. Periodic finite element unit cell models are utilized for this task, which offer the big advantage of a homogeneous load introduction to the structure. The finite element models are found to be well suited for all kinds of buckling predictions. Different uni- and bi-axial loadings are considered as well as influences of core height, core material, core geometry, and facesheet thickness are investigated. Finally, a new analytical approach is introduced for the unexpected core cell wall buckling under in-plane compression of the sandwich, which predicts the critical load very accurately.

keyword: Sandwich Buckling, Wrinkling, Dimpling, Periodic Unit Cells, Finite Element Method

1 Introduction

Sandwich structures exhibit very high structural efficiencies (ratio of strength or stiffness to weight) and, therefore, are of interest in the use of aerospace structures. A sandwich consists of two thin load bearing facesheets glued on a lightweight core that prevents the facesheets from buckling individually. Quasi homogeneous cores (e.g., made of foam) and cellular cores (e.g., honeycomb cores) respectively, are typically used.

Failure modes of sandwich structures, as stated in standard literature, are: global buckling, shear crimping, facesheet wrinkling, facesheet dimpling, face/core yielding, core-face debonding (Plantema (1966), Zenkert (1995)).

Comparisons of analytical and experimental results (Ley, Lin, and Uy (1999)) show poor correlations if honeycomb cores are used. Sandwiches with honeycomb cores show, besides other failure modes, facesheet dimpling, which comes from the non-continuous facesheet support by the core. This non-continuous support influences also the wrinkling behavior of the facesheets. In Lamberti, Venkataraman, Haftka, and Johnson (2003) it is stated that one wrinkling half wave has to go over at least two honeycomb cells in order to obtain reliable analytical estimations based on continuous support assumptions. This fact might be the reason for the poor agreement between analytical and experimental results in Ley, Lin, and Uy (1999).

The present study aims to highlight the above mentioned problems in the transition zone where one buckling half wave length is smaller than the length of two honeycomb cells. Analytical and finite element analyses are applied. The Finite Element Method (FEM) Bathe (1996) is used for numerical instead of physical experiments. The advantage of this approach lies in the avoidance of complex, not very reliable and expensive experiments as well as in the possibility of investigating new core geometries, which are not realized yet.

Our specific objectives are to: (1) introduce a new type of finite element model for the problem - namely periodic unit cell models, (2) investigate different loading conditions (uni-axial compression, bending, bi-axial compression), (3) compute influences of different facesheet thicknesses, core heights, core materials, (4) compare different cell geometries (hexagonal, square) of a structured core.

One of the novelties of this work is the usage of periodic finite element unit cell models for studying all kind

[1] Institute of Lightweight Design and Structural Biomechanics, Vienna University of Technology, A-1040 Vienna, Austria

of sandwich failure modes (global buckling, wrinkling, dimpling, yielding), instead of FEM models of sandwich specimens. This approach requires complex boundary conditions for proper load introduction (see Léotoing, Drapier, and Vautrin (2004)). Furthermore, a new analytical formula is introduced for cell wall buckling under multi-axial in-plane compression loading.

2 Methods

In this section the homogenization as well as the analytical buckling formulae for different sandwich failure modes - global buckling, facesheet wrinkling of sandwiches with thin and thick cores, facesheet dimpling, face/core yielding, cell wall buckling under multi-axial in-plane compression - are considered, and the periodic finite element models are described.

In the following critical membrane loads per unit width of the sandwich are denoted as N and M, whereas critical loads per unit width of a single facesheet are denoted as F. It is assumed that this membrane loads are sufficiently homogeneous.

If not denoted otherwise, uni-axial loading is assumed in the analytical expressions.

2.1 Homogenization

The constitutive law for an effective plane periodic media in terms of classical lamination theory can be written as (see Jones (1999):

$$\begin{pmatrix} \underline{\boldsymbol{N}}^{\mathrm{h}} \\ \underline{\boldsymbol{M}}^{\mathrm{h}} \end{pmatrix} = \begin{pmatrix} \underline{\underline{\boldsymbol{A}}}^{\mathrm{h}} & \underline{\underline{\boldsymbol{B}}}^{\mathrm{h}} \\ \underline{\underline{\boldsymbol{B}}}^{\mathrm{h}} & \underline{\underline{\boldsymbol{D}}}^{\mathrm{h}} \end{pmatrix} \begin{pmatrix} \overline{\underline{\boldsymbol{\varepsilon}}}^{\mathrm{h}} \\ \overline{\underline{\boldsymbol{\chi}}}^{\mathrm{h}} \end{pmatrix} \tag{1}$$

with the resultant forces

$$\underline{\boldsymbol{N}}^{\mathrm{h}} = (N_{11}\ N_{22}\ N_{12})^{\mathrm{T}},$$

the resultant moments

$$\underline{\boldsymbol{M}}^{\mathrm{h}} = (M_{11}\ M_{22}\ M_{12})^{\mathrm{T}},$$

the reference-surface strains

$$\overline{\underline{\boldsymbol{\varepsilon}}}^{\mathrm{h}} = (\mathcal{E}_{11}\ \mathcal{E}_{22}\ 2\mathcal{E}_{12})^{\mathrm{T}},$$

and the reference-surfacde curvatures

$$\overline{\underline{\boldsymbol{\chi}}}^{\mathrm{h}} = (-\chi_{11}\ -\chi_{22}\ -2\chi_{12})^{\mathrm{T}}.$$

If the homogenization problem is solved by the Finite Element Method (FEM) these quantities have to be related to nodal forces and nodal displacement. The homogenized stiffness matrices $\underline{\underline{\boldsymbol{A}}}^{\mathrm{h}}$, $\underline{\underline{\boldsymbol{B}}}^{\mathrm{h}}$ and $\underline{\underline{\boldsymbol{D}}}^{\mathrm{h}}$ can than be computed from FEM results.

Following the theory of homogenization (Suquet (1987)) periodic boundary conditions (BCs) have to be applied on the boundaries of an appropriate FE-unit cell (as shown in Figure 1) in order to ensure that for each undeformed and deformed configuration the translated unit cells fit with each other. Considering the periodic BCs, the macroscopic displacement field within the unit cell is completely defined by the displacements of characteristic points, so called master nodes (A, A^+, B, B^+, and 0, 0^+ in Figure 1).

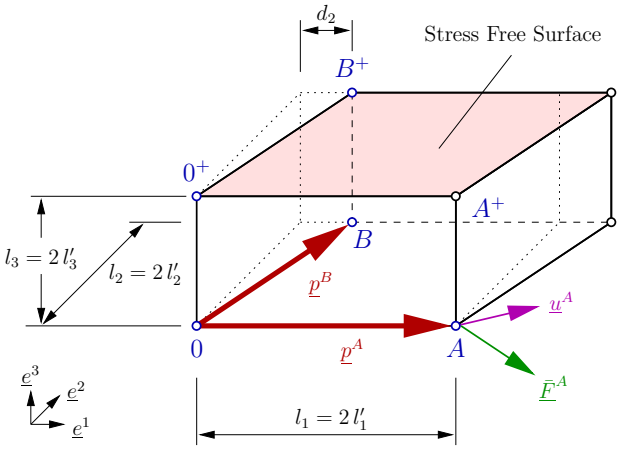

Figure 1 : Unit cell definition for a plane periodic media (for a rectangular cell: $d_2 = 0$)

Consequently, the distributed loads acting along the boundary of the unit cell are condensed to concentrated nodal forces at the master nodes (e.g. $\underline{\bar{F}}^A$, $\underline{u}^A$ in Figure 1).

The relations between these nodal quantities and the quantities in the homogenized constitutive law (Equation (1)) start with the definition of the characteristic rotations and displacements (for similar equations see Anthoine (1995), Hohe (2003)). The rotations R, S and twisting T of the unit cell are given by:

$$R_1 = -\frac{1}{2\,l_3'}\Big((u_2^{A^+} - u_2^{A}) - (u_2^{0^+} - u_2^{0})\Big)$$

$$R_2 = \frac{1}{2\,l_3'}\Big((u_1^{A^+} - u_1^{A}) - (u_1^{0^+} - u_1^{0})\Big)$$

$$
\begin{aligned}
R_3 &= \frac{1}{2\,l_3'}\Big((u_3^{A^+} - u_3^A) - (u_3^{0^+} - u_3^0)\Big) = 0\\
S_1 &= -\frac{1}{2\,l_3'}\Big((u_2^{B^+} - u_2^B) - (u_2^{0^+} - u_2^0)\Big)\\
S_2 &= \frac{1}{2\,l_3'}\Big((u_1^{B^+} - u_1^B) - (u_1^{0^+} - u_1^0)\Big)\\
S_3 &= \frac{1}{2\,l_3'}\Big((u_3^{B^+} - u_3^B) - (u_3^{0^+} - u_3^0)\Big) = 0\\
T &= -\frac{1}{4\,l_1'\,l_3'}\Big((u_2^{A^+} - u_2^A) - (u_2^{0^+} - u_2^0)\Big).
\end{aligned}
\tag{2}
$$

Note that $R_3 = S_3 = 0$ are zero constants in order to ensure that translated unit cells fit with each other.

The connections of the master node displacements and the characteristic translations (U, V) are:

$$
\begin{aligned}
U_1 &= \frac{1}{2}\Big((u_1^{A^+} + u_1^A) - (u_1^{0^+} + u_1^0)\Big)\\
U_2 &= \frac{1}{2}\Big((u_2^{A^+} + u_2^A) - (u_2^{0^+} + u_2^0)\Big)\\
U_3 &= \frac{1}{2}\Big((u_3^{A^+} + u_3^A) - (u_3^{0^+} + u_3^0)\Big) + (R_1 - R_2\,\frac{d_2}{2l_2'})\,l_2'\\
V_1 &= \frac{1}{2}\Big((u_1^{B^+} + u_1^B) - (u_1^{0^+} + u_1^0)\Big)\\
V_2 &= \frac{1}{2}\Big((u_2^{B^+} + u_2^B) - (u_2^{0^+} + u_2^0)\Big)\\
V_3 &= \frac{1}{2}\Big((u_3^{B^+} + u_3^B) - (u_3^{0^+} + u_3^0)\Big) - S_2\,l_1'.
\end{aligned}
\tag{3}
$$

The third and sixth equations are thickness compatibility conditions.

Using the definitions of Equation (2) and Equation (3) the homogenized strains and curvatures follow from (see Anthoine (1995)):

$$
\begin{aligned}
\mathcal{E}_{11} &= \frac{U_1}{2\,l_1'}\\
\mathcal{E}_{21} &= \frac{U_2}{2\,l_1'}\\
\mathcal{E}_{12} &= \frac{V_1}{2\,l_2'} - \frac{U_1\,d_2}{4\,l_1'\,l_2'}\\
\mathcal{E}_{22} &= \frac{V_2}{2\,l_2'} - \frac{U_2\,d_2}{4\,l_1'\,l_2'}
\end{aligned}
\tag{4}
$$

$$
\begin{aligned}
\chi_{11} &= -\frac{R_2}{2\,l_1'}\\
\chi_{21} &= T\\
\chi_{12} &= T\\
\chi_{22} &= \frac{S_1}{2\,l_2'} - \frac{T\,d_2}{2\,l_2'}
\end{aligned}
\tag{5}
$$

The above derivations may also be written in the form of:

$$
\underline{\underline{\boldsymbol{U}}} = \underline{\underline{\boldsymbol{\mathcal{E}}}} \cdot \underline{\underline{\boldsymbol{P}}} \qquad \longleftrightarrow \qquad U_{ij} = \mathcal{E}_{im}\,P_{mj}\,, \tag{6}
$$

where $\underline{\underline{\boldsymbol{U}}}$ is the generalized master node displacement tensor, $\underline{\underline{\boldsymbol{\mathcal{E}}}}$ is the homogenized strain and $\underline{\underline{\boldsymbol{P}}}$ is the generalized periodicity tensor containing the unit cell geometry l_1, l_2 and d_2. and in extended form as (for more details see Pahr (2003)):

$$
\begin{pmatrix} U_1 & V_1 \\ U_2 & V_2 \end{pmatrix} = \begin{pmatrix} \mathcal{E}_{11} & \mathcal{E}_{12} \\ \mathcal{E}_{21} & \mathcal{E}_{22} \end{pmatrix} \cdot \begin{pmatrix} p_1^A & p_1^B \\ p_2^A & p_2^B \end{pmatrix} \tag{7}
$$

A similar relation is obtained for the curvatures as:

$$
\underline{\underline{\boldsymbol{R}}} = \underline{\underline{\boldsymbol{\chi}}} \cdot \underline{\underline{\boldsymbol{P}}} \qquad \longleftrightarrow \qquad R_{ij} = \chi_{im}\,P_{mj}\,, \tag{8}
$$

and in extended form as:

$$
\begin{pmatrix} -R_2 & -S_2 \\ R_1 & S_1 \end{pmatrix} = \begin{pmatrix} \chi_{11} & \chi_{12} \\ \chi_{21} & \chi_{22} \end{pmatrix} \cdot \begin{pmatrix} p_1^A & p_1^B \\ p_2^A & p_2^B \end{pmatrix} \tag{9}
$$

The generalized resultant forces $\underline{\underline{\boldsymbol{N}}}$ are obtained by integration of the stresses through the thickness which yields:

$$
\underline{\underline{\boldsymbol{N}}} = \frac{l_3}{2V}\left(\underline{\underline{\overline{\boldsymbol{F}}}} \cdot \underline{\underline{\boldsymbol{P}}}^{\mathrm{T}} + \underline{\underline{\boldsymbol{P}}} \cdot \underline{\underline{\overline{\boldsymbol{F}}}}^{\mathrm{T}}\right) \tag{10}
$$

with

$$
\underline{\underline{\overline{\boldsymbol{F}}}} = \begin{pmatrix} \overline{F}_1^A & \overline{F}_1^B \\ \overline{F}_2^A & \overline{F}_2^B \end{pmatrix} \text{ and } \underline{\underline{\boldsymbol{N}}} = \begin{pmatrix} N_{11} & N_{12} \\ N_{21} & N_{22} \end{pmatrix}, \tag{11}
$$

where $\underline{\underline{\overline{\boldsymbol{F}}}}$ is the generalized master node force tensor. V is the volume of the unit cell and "$\cdot$" stands for the dot product. That means if $\underline{\underline{\boldsymbol{\mathcal{E}}}}$ is given (strain controlled loading) $\underline{\underline{\boldsymbol{U}}}$ follows from Equation (6), $\underline{\underline{\overline{\boldsymbol{F}}}}$ is calculated by using FE-analyses and $\underline{\underline{\boldsymbol{N}}}$ is computed from Equation (10).

Similarly a generalized resultant moment $\underline{\underline{\boldsymbol{M}}}$ can be found as:

$$
\underline{\underline{\boldsymbol{M}}} = \frac{l_3\,l_3}{2V}\left(\Delta\underline{\underline{\boldsymbol{F}}} \cdot \underline{\underline{\boldsymbol{P}}}^{\mathrm{T}} + \underline{\underline{\boldsymbol{P}}} \cdot \Delta\underline{\underline{\boldsymbol{F}}}^{\mathrm{T}}\right) \tag{12}
$$

with

$$\Delta\underline{\underline{\boldsymbol{F}}} = \begin{pmatrix} \Delta F_1^A & \Delta F_1^B \\ \Delta F_2^A & \Delta F_2^B \end{pmatrix} = \begin{pmatrix} F_1^{A+} - F_1^A & F_1^{B+} - F_1^B \\ F_2^{A+} - F_2^A & F_2^{B+} - F_2^B \end{pmatrix}, \tag{13}$$

where for strain controlled loading Equation (8) and Equation (12) is needed. Finally $\underline{\underline{\boldsymbol{N}}}$, $\underline{\underline{\boldsymbol{M}}}$, $\underline{\underline{\boldsymbol{\mathcal{E}}}}$, $\underline{\underline{\boldsymbol{\chi}}}$ are used in Equation (1), and $\underline{\underline{\boldsymbol{A}}}^{\mathrm{h}}$, $\underline{\underline{\boldsymbol{B}}}^{\mathrm{h}}$, $\underline{\underline{\boldsymbol{D}}}^{\mathrm{h}}$ are computed.

The equations for stress controlled loading look similar. There the master nodal forces follow from given resultant forces as:

$$\overline{\underline{\underline{\boldsymbol{F}}}} = \frac{V}{l_3}\underline{\underline{\boldsymbol{N}}} \cdot (\underline{\underline{\boldsymbol{P}}}^{\mathrm{T}})^{-1} \tag{14}$$

$$\Delta\underline{\underline{\boldsymbol{F}}} = \frac{V}{l_3 l_3}\underline{\underline{\boldsymbol{M}}} \cdot (\underline{\underline{\boldsymbol{P}}}^{\mathrm{T}})^{-1} \tag{15}$$

The required relation between master node displacements and homogenized strains/curvatures follows directly from the inverse of Equation (6)/(8) as:

$$\underline{\underline{\boldsymbol{\mathcal{E}}}} = \frac{1}{2}\left(\underline{\underline{\boldsymbol{U}}} \cdot \underline{\underline{\boldsymbol{P}}}^{-1} + (\underline{\underline{\boldsymbol{P}}}^{-1})^{\mathrm{T}} \cdot \underline{\underline{\boldsymbol{U}}}^{T}\right) \tag{16}$$

and

$$\underline{\underline{\boldsymbol{\chi}}} = \frac{1}{2}\left(\underline{\underline{\boldsymbol{R}}} \cdot \underline{\underline{\boldsymbol{P}}}^{-1} + (\underline{\underline{\boldsymbol{P}}}^{-1})^{\mathrm{T}} \cdot \underline{\underline{\boldsymbol{R}}}^{T}\right). \tag{17}$$

For the computation of the homogenized stiffness matrices six independent load cases are needed and the periodic BCs have to be applied on the FE unit cell model. These tasks are done by the house software UCTOOL. The homogenization problem is solved by the commercial FE software ABAQUS.

2.2 Global Buckling

The problem of global buckling of a sandwich beam is dealt with in the classical sandwich literature (e.g. Plantema (1966)):

$$\frac{1}{P^{\mathrm{G}}} = \frac{1}{P^{\mathrm{E}}} + \frac{1}{P^{\mathrm{S}}}, \tag{18}$$

where P^{E} denotes the Euler buckling load (with neglection of the core stiffness):

$$P^{\mathrm{E}} = \frac{\pi^2 E_{\mathrm{f}} J}{l_K^2} \qquad J = 2 t_{\mathrm{f}} b \left(\frac{h_{\mathrm{c}}}{2}\right)^2 \tag{19}$$

and P^{S} is the shear crimping load per unit width (with neglection of the transverse shear stiffness of facesheets and assumption of relatively thin facesheets):

$$P^{\mathrm{S}} = \overline{G} b h_{\mathrm{c}}. \tag{20}$$

Here $\overline{G}$ denotes the effective transverse core shear modulus ($\overline{G}_{xz}$ or $\overline{G}_{yz}$), h_{c} the core height, b the width of the sandwich, t_{f} the facesheet thickness, E_{f} the facesheet Young's modulus, and l_K the buckling length. The material parameters for all applied cores and facesheets can be found in Table 1 and Table 2. The core values (Table 1) are similar to those of core material data sheets, although they are based on FE computations.

Table 1 : Honeycomb core dimensions and material parameters

Param.	Description	Alu	Nomex	Unit
SW	cell size	4.7625	4.7625	mm
h_{c}	core height	10…50	10…50	mm
t_{c}	cell wall thickness	0.05	0.05	mm
E_{c}	Young's modulus of core	60000.	1600.	MPa
ν_{c}	Poisson ratio of core	0.3	0.3	-
σ_Y	wall yield stress of core	220.	220.	MPa
$\overline{E}_x$ *	eff. Young's mod. of core	0.94	0.0251	MPa
$\overline{E}_y$ *	eff. Young's mod. of core	0.94	0.0251	MPa
$\overline{E}_z$ *	eff. Young's mod. of core	1679.	44.794	MPa
$\overline{G}_{yz}$ *	eff. shear mod. of core	242.47	6.4658	MPa
$\overline{G}_{xz}$ *	eff. shear mod. of core	363.83	9.7021	MPa
$\overline{G}_{xy}$ *	eff. shear mod. of core	0.562	0.01499	MPa
$\overline{\nu}_{yz}$ *	eff. Poisson ratio of core	1.7E-4	1.67E-4	-
$\overline{\nu}_{xz}$ *	eff. Poisson ratio of core	1.7E-4	1.67E-4	-
$\overline{\nu}_{xy}$ *	eff. Poisson ratio of core	0.999	0.999	-
k_x^{thick} *	foundation stiffness†	364.569	9.728	MPa
k_y^{thick} *	foundation stiffness†	364.217	9.719	MPa

* computed with spatially periodic finite element models
† based on Vonach and Rammerstorfer (2001)

Table 2 : Facesheet dimensions and material parameters

Param.	Description	Alu	Steel	Unit
t_{f}	facesheet thickness	0.01…0.5	0.01…0.5	mm
E_{f}	Young's modulus	60000.	210000.	MPa
ν_{f}	Poisson's ratio	0.3	0.3	-
σ_Y	yield stress	220.	400.	MPa

2.3 Wrinkling

Wrinkling is a common local stability problem, which leads to the loss of stiffness and to a subsequent catas-

trophic failure. The literature divides the wrinkling problem into two different cases. The first case is the "thick sandwich" case, where it is assumed that the sandwich thickness is big enough to avoid interaction between the two facesheets. The second case is the "thin sandwich" case, where the facesheets interact. Both cases have been compared and discussed more closely in Ley, Lin, and Uy (1999), Yusuff (1955) and are used in standard sandwich literature (Plantema (1966), Zenkert (1995), Allen (1969)).

In very simple approaches thin cores are practically modelled as plates on an elastic foundation (Winkler foundation). Assuming a symmetric wrinkling pattern the critical compression load per unit width of a facesheet is given by (Yusuff (1955),Allen (1969)):

$$F^{\text{Wrink,thin}} = 2t_{\text{f}}\sqrt{\frac{E_{\text{f}}\overline{E}_z t_{\text{f}}}{6\,(1-\nu_{\text{f}}^2)\,h_{\text{c}}}}\,, \tag{21}$$

where $\overline{E}_z$ is the effective Young's modulus of the core in thickness direction (z-direction), which are given in Table 1. Equation (21) assumes a symmetric sandwich (i.e. geometry, material, load, and solution are symmetric with respect to the mid-plane). Anti-symmetric buckling modes, bending loading, etc. are not taken into account, a fact which leads to wrong results for many cases. A more general approach is proposed in Vonach and Rammerstorfer (2001), with which all these problems are solved and which is applicable to sandwich beams, plates, and shells of arbitrary configurations with respect to anisotropy of core and facesheet materials. However, in order to find the relevant solution an optimization problem has to be solved.

The asymptotic solution of the general approach in Vonach and Rammerstorfer (2001) is used for the buckling load predictions of thick cores. The solution (critical compression load per unit width of a facesheet) is then given directly as:

$$F^{\text{W,thick}} = 0.85\,t_{\text{f}}\sqrt[3]{E_{\text{f}}\,(k^{\text{thick}})^2} \qquad \text{if} \quad \nu_{\text{f}} = 0.3\,. \tag{22}$$

The foundation stiffness k^{thick}=$k^{\text{thick}}(\overline{E}_z\,\overline{G}_{xz},\overline{E}_x\ldots)$ is computed by a set of formulae which are taken from Vonach (2001) (see Table 1). Equation (22) is similar to the classical approach for thick cores, i.e., $F^{\text{W,thick,class}} = 0.85\,t_{\text{f}}\sqrt[3]{E_{\text{f}}\overline{E}_z\,\overline{G}_{xz}}$ (ν_{f}=0.3, see Ley, Lin, and Uy (1999)) but includes the influence of the in-plane core stiffness ($\overline{E}_x$), which is disregarded in the classical approach.

The critical wrinkling load per unit width of the facesheet can finally taken as:

$$F^{\text{W}} = \max\left(F^{\text{W,thick}},\, F^{\text{W,thin}}\right). \tag{23}$$

2.4 Dimpling

Dimpling as a local mode of instability occurs only in the case of cellular cores as, for example, honeycomb cores. Many design approaches regarding dimpling are available (e.g. Plantema (1966), Norris and Kommers (1950), Department of Defense (1968)). Here, the formula for dimpling load prediction taken from the US Military Handbook Department of Defense (1968) is used, which is also suggested in Ley, Lin, and Uy (1999). There the critical compression load per unit width of a facesheet is given as:

$$F^{\text{D}} = \frac{2E_{\text{f}}t_{\text{f}}}{1-\nu_{\text{f}}^2}\left(\frac{t_{\text{f}}}{\frac{SW}{2}}\right)^2. \tag{24}$$

SW corresponds to the cell size (see Figure 2).

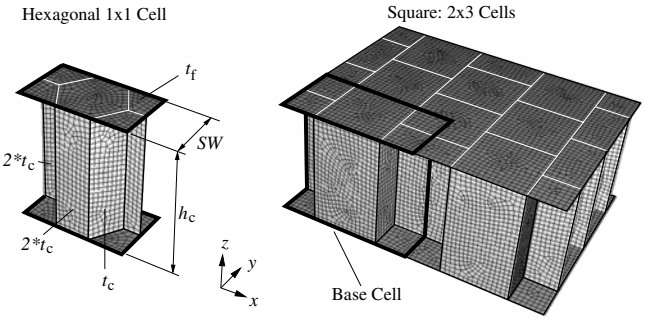

Figure 2 : Finite element model examples: Hexagonal 1×1 cell model (right, h_{c}=10 mm, SW=4.7526 mm) and rectangular (square) 2×3 cell model (left).

2.5 Cell Wall Buckling (under in-plane compressive loading of the sandwich)

Finite element computations performed for the present work have show that a further local instability mode under in-plane compression can appear, namely cell wall buckling. For an analytical prediction of this instability a new failure model is introduced. The development of the model starts with a look at the deformation pattern of a honeycomb core. Figure 3 shows FE results of a 1×2 unit cell under compression loading.

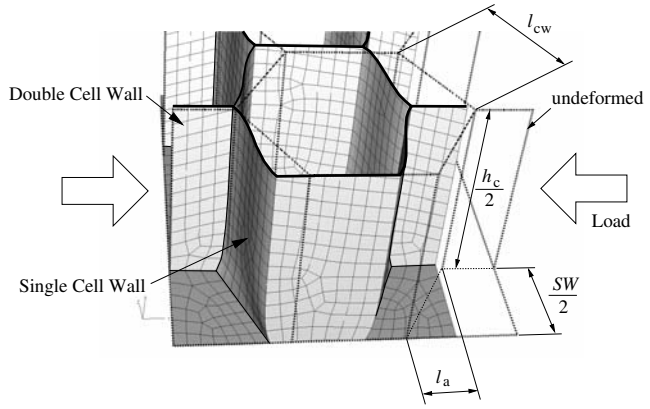

Figure 3 : Undeformed (dashed line) and deformed shape, respectively, of an 1×2 unit cell (upper part not shown).

One can see that the deviation of the regular core displacement decays fast from the facesheet to the mid plane (=cut plane) of the sandwich. These observations lead to the following proposed model for cell wall buckling considerations:

Step 1: Compute the overall displacement of a sandwich unit cell as shown in Figure 3. Classical Lamination Theory (CLT, see Jones (1999)) is used for this task. The core is modelled as a homogenized material with effective properties as shown in Table 1. These values are computed by spatial periodic finite element unit cell models, i.e., without modelling the facesheets (see Daxner (2003), Pahr (2003)). These FEM models are similar to the plane periodic models as described later in this section. The obtained overall displacements are denoted with ${}^1u_x$ and ${}^1u_y$.

Step 2: The "double cell wall" ($t = 2t_c$) is assumed to carry the effective core stress. The (rather small) displacements of these walls are computed and the relevant component is denoted as ${}^2u_x$.

Step 3: The "single cell wall" ($t = t_c$) is loaded with the displacement from step 1 minus the displacement from step 2 as:

$$\Delta u = \sqrt{\left(l_a + {}^1u_x - {}^2u_x\right)^2 + \left(\frac{SW}{2} + {}^1u_y\right)^2} - l_{cw} \tag{25}$$

and the cell wall stress is obtained from:

$$\sigma^{CW} = E_c \frac{\Delta u}{l_{cw}}, \tag{26}$$

where l_{cw} and l_a are characteristic lengths (see Figure 3).

Step 4: This cell wall stress is assumed to be constant within the considered cell wall and is compared to the critical buckling stress for plate buckling (uniaxial compression):

$$\sigma^{PB} = k E_c \left(\frac{t_c}{l_{cw}}\right)^2, \tag{27}$$

in order to obtain the critical load multiplier for cell wall buckling from:

$$\lambda = \frac{\sigma^{PB}}{\sigma^{CW}}. \tag{28}$$

The parameter k is the plate buckling factor which can be taken from Plantema (1966) or Zenkert (1995). It depends on the ratio h_c/l_{cw} as well as on the clamping conditions along the four edges. In the considered case the clamping conditions are something inbetween fully clamped (fixed) and simply supported (rotational free). It is found (see section 3) that a value of k inbetween the ones corresponding to these two extreme values is a good choice.

The accuracy of the proposed model depends on how good the mean stress in the cell wall is captured by the analytical approach. Otherwise the factor k becomes an unphysical fitting parameter. This validation is done in the result section.

2.6 Facesheet Yielding

Von Mises plasticity is used for predicting facesheet yielding. In the analytical approach the actual von Mises stress is compared to the face yield stress, where the current stress state within the facesheet is obtained from CLT. Thus multi-axial loading can be taken into account very simply.

In the FEM approach the von Mises stresses are averaged within the different sections (facesheets, core materials with different thicknesses). These average stresses are compared to the yield stress of the considered material in order to obtain a critical load multiplier.

2.7 Multi-axial Loading

A sandwich plate or shell, as considered in the present work, can be loaded in-plane by membrane forces N_{xx},

N_{yy}, N_{xy} and moments M_{xx}, M_{yy}, M_{xy}, respectively. Here, for yielding and cell wall buckling the multi-axial stress state is computed by using CLT. With respect to wrinkling and dimpling the membrane forces in the facesheets can be estimated by:

$$F_{ij}^{\mathrm{N}} = \frac{N_{ij}}{2}$$
$$F_{ij}^{\mathrm{M}} = \frac{M_{ij}}{h_{\mathrm{c}}} \tag{29}$$

if the in-plane stiffness of the core is neglected. For example, if the critical load multipliers λ of a sandwich (t_f=0.01 mm, h_c =10mm, aluminum facesheets, hexagonal aluminum core, compressive N_{xx} loading) are computed with and without considering the in-plane stiffness of the core, respectively, a difference of 0.64% is found, which verifies this neglection.

In the case of wrinkling and dimpling an interaction formula (taken from Ley, Lin, and Uy (1999)) is used to obtain the critical load multiplier λ of the sandwich under both membrane and bending loads ($F_{xy}^{\mathrm{N}} = F_{xy}^{\mathrm{M}} = 0$):

$$\frac{1}{\lambda} = \sqrt[p]{\left(\frac{F_{xx}^{\mathrm{N}} + F_{xx}^{\mathrm{M}}}{F_{xx}^{\mathrm{W,D}}}\right)^p + \left(\frac{F_{yy}^{\mathrm{N}} + F_{yy}^{\mathrm{M}}}{F_{yy}^{\mathrm{W,D}}}\right)^p}, \tag{30}$$

where $F_{xx}^{\mathrm{W,D}}$, $F_{yy}^{\mathrm{W,D}}$ are the critical wrinkling and dimpling loads from Equation (23) and Equation (24), respectively, and p is a coefficient which is chosen as p=3 in Ley, Lin, and Uy (1999).

2.8 Finite Element Modelling

Finite element unit cell simulations are performed in order to validate the approximating analytical approaches and to get more insight into the instability phenomena.

The proposed periodic finite element models show the following characteristics:

- Three-dimensional shell models of the sandwich (see Figure 2) composed of quadratic 8 noded shell elements are applied.
- The smallest FE model size is shown in Figure 2, left. Larger FE model sizes are denoted with "$n_x \times n_y$", where n_x and n_y are the number of base cells in x and y direction, respectively. For example, Figure 2 (right) shows a 2×3 cell model.
- The core geometry can be hexagonal (Figure 2, left) or square (Figure 2, right). Other possible core geometries are not investigated in this paper.
- The cell wall thickness for walls normal to the y-axis is $2t_{\mathrm{c}}$ due to the manufacturing process. The other walls have a thickness of t_{c}.
- Plane periodic boundary conditions are applied along corresponding edges (see Pahr (2003), Hohe (2003)).
- Loads can be membrane forces N_{ij}, moments M_{ij} or a combination of forces and moments. Figure 4 shows the deformation pattern for a 1×2 cell model under the six possible unit load cases. The loads are unit loads with a value of "1", i.e. the critical load multiplier λ is equal to the critical load of the sandwich.

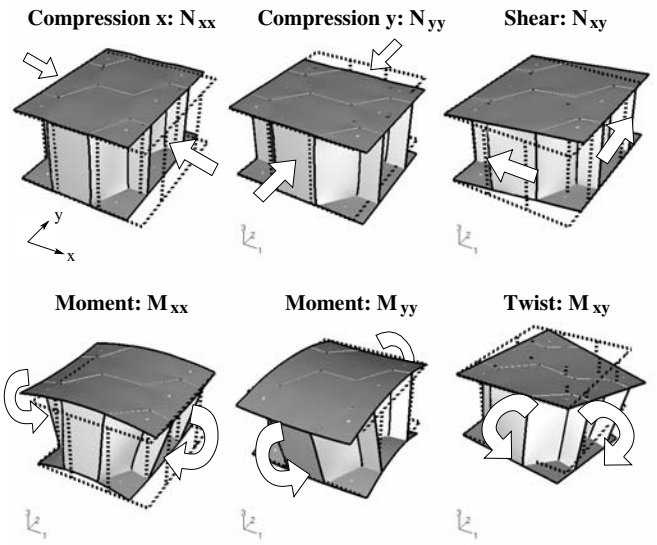

Figure 4 : Deformation pattern of different load cases on a unit cell: Compression 2×, Shear, Moments 2×, Twist. Dashed lines represent the undeformed state.

- Analysis steps are a pre-load step followed by a classical linear buckling step. Investigations of different pre-load levels as well as geometric nonlinear analyses have shown that the considered models are not sensitive to geometric non-linearities. However it should be mentioned, that possible imperfection sensitivities are not considered in the present work.

- The models are generated by the pre-processor ABAQUS/CAE and solved with ABAQUS/Standard (ABAQUS (2005)). The post-processing is done by a user script written in PYTHON.
- Figure 2 shows typically used mesh density. Finer meshes have shown that this mesh is sufficiently fine.
- The global buckling length l_k in the analytical models corresponds to the size of the FE unit cells.
- The number of core cells along the x and y direction depends on the problem (wrinkling, dimpling, global buckling) which is to be solved.

In contrast to previous works (e.g. Léotoing, Drapier, and Vautrin (2004)) a special treatment of the load introduction region is not needed in the case of periodic FE models. Of course, a critical point is the periodicity. This means that the geometry, material, load and solution has to be periodic. The latter is fulfilled in dimpling, cell wall buckling, and yielding analyses. For dimpling a 1×2 cell model is found to be sufficient. For wrinkling and global buckling modes larger models have to be utilized and the obtained buckling pattern is approximative. Nevertheless, if a sufficiently large number of cells is chosen properly (see Figure 13) than the error in the results is found to be negligibly small (see result section).

3 Results

The failure behavior of a sandwich structure under different loading conditions (Figures 5 - 7) shows dimpling, facesheet yielding, and cell wall buckling. The aluminum core of the specifically considered sandwich has a constant thickness of h_c=10 mm. The aluminum facesheets have thicknesses ranging from 0.01 to 0.5 mm. For all cases a very good agreement between the analytical and the finite element results is found. A 1×2 unit cell size is found to be sufficiently large in the considered case, if global buckling is not considered.

Under uni-axial compression of the sandwich (Figure 5) dimpling and cell wall buckling are the critical failure modes, where wrinkling and facesheet yielding does not occur. Global buckling (in this case mainly shear crimping) is also not critical due to the small considered unit cell, i.e., small bucking length. Dimpling is critical for a facesheet thickness lower than 0.1 mm and shows a full dimpling wave over one honeycomb cell (Figure 5, A). For cell wall buckling predictions a constant plate buckling factor of k =2.9 has been seen to be appropriate and one full buckle half wave is visible within the buckled cell walls (Figure 5, B).

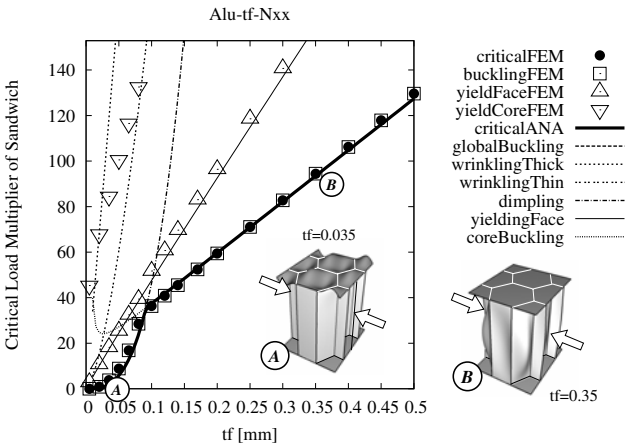

Figure 5 : Critical load multiplier λ over facesheet thickness of an aluminum (facesheet material) - aluminum (hexagonal core material) sandwich (h_c=10 mm) under uni-axial compression N_{xx}. Lines are analytical results, symbols are FE results. The thick line and solid circles represent the critical load multipliers.

Bending moments (Figure 6) lead to dimpling for small facesheets thicknesses and to facesheets yielding for

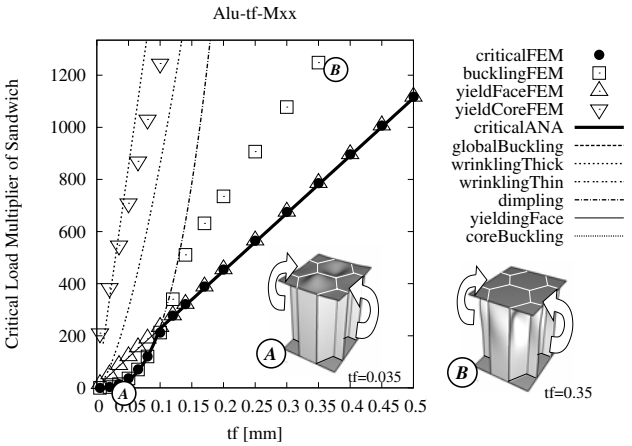

Figure 6 : Critical load multiplier λ over facesheet thickness of a hexagonal aluminum-aluminum sandwich (h_c=10 mm) under uni-axial bending M_{xx}.

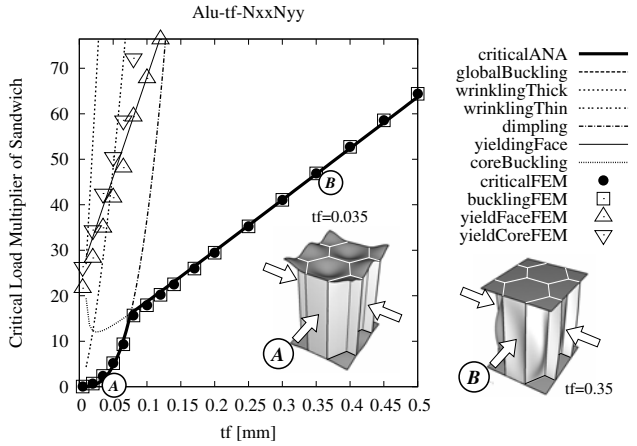

Figure 7 : Critical load multiplier λ over facesheet thickness of a hexagonal aluminum-aluminum sandwich (h_c=10 mm) under bi-axial compression $\frac{N_{xx}}{N_{yy}}$=1.

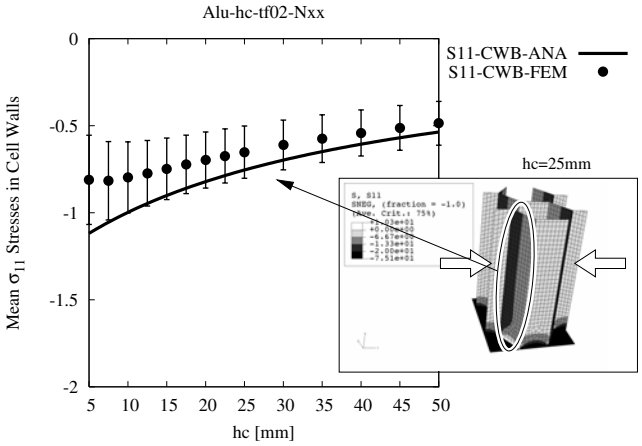

Figure 8 : Mean compression stress in the "single" cell walls ($t = t_c$) due to loading N_{xx} = 1N/mm as a function of the core height (h_c=5...50 mm). The solid symbols represent the averaged FEM stresses within the cell walls, the error bars are the standard deviation of the FEM stresses, and the solid line show the cell wall stresses obtained from the analytical model. The stress field is also shown for the lower half of an 1×2 cell.

larger thicknesses. Different dimpling patterns (Figure 6, A) and cell wall buckling patterns (Figure 6, B) are visible for small and large core thicknesses, respectively.

A bi-axially loaded sandwich (Figure 7) shows a behavior similar to the uni-axially loaded sandwich. However a reduced buckling load is appearant. The buckling interaction formula (Equation (30)) works well for this type of bi-axial loading. The good agreement between the analytical, and finite element results for cell wall buckling (open squares in Figure 7) and facesheets yielding (open triangles) is only reached if the proposed CLT approach is used for the analytical computations, i.e., if the core stiffness is taken into account. The buckling factor k is the same as for uni-axial loading, where $k = 2.9$.

For the verification of the cell wall buckling model, FE and analytical results of the mean "single" cell wall stress ($t = t_c$) are compared (see Figure 8). They agree very well for thicker cores. The solid line in Figure 8 shows the analytical results calculated with the introduced cell wall buckling model. The finite element results for these stresses in the considered case are averaged and the standard deviation is computed from these stresses (solid symbols and error bars in Figure 8). The difference in the computed mean stresses ranges from 17.0...3.6% for h_c=10...50 mm.

Based on this validation, cell wall buckling predictions (Figure 9) show, as expected, that the critical load is a function of the core height. The considered aluminum-aluminum honeycomb sandwich has a facesheet thick-

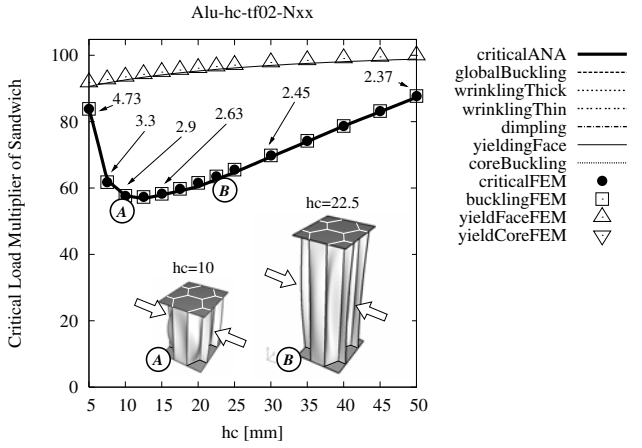

Figure 9 : Critical load multiplier λ over core thickness of a hexagonal aluminum-aluminum sandwich (t_f=0.2 mm) under uni-axial compression N_{xx}. The critical buckling failure is cell wall buckling. The numbers along the critical line are the plate buckling factors k.

ness of 0.2 mm in order to result in cell wall buckling as critical failure mode. The good agreement of both, analytical and computational, predictions is obtained if the plate buckling coefficient is taken from buckling factor diagrams of plates under compression for different

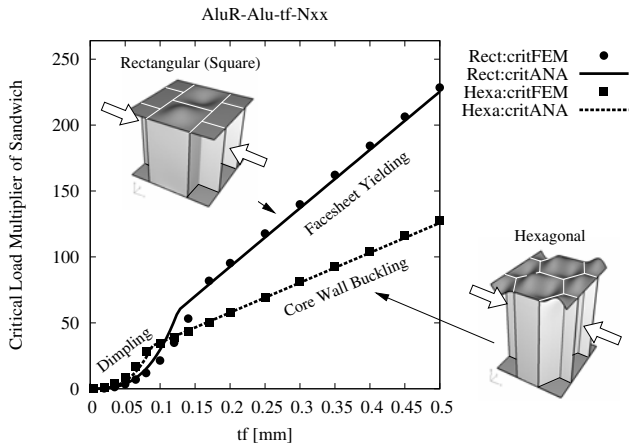

Figure 10 : Critical load multiplier λ over facesheet thickness of aluminum-aluminum sandwich (h_c=10 mm) with hexagonal and rectangular cores (h_c=10 mm) under uni-axial compression N_{xx}. Both sandwiches show the same effective core density.

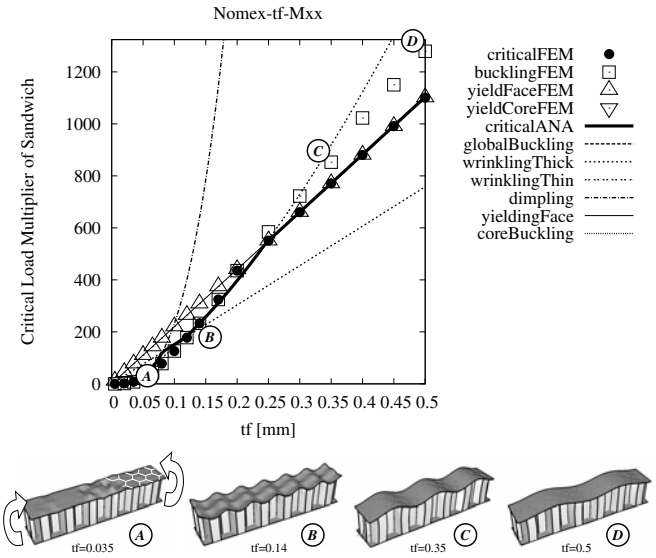

Figure 11 : Critical load multiplier λ over facesheet thickness of a aluminum (facesheet) - Nomex (hexagonal core) sandwich (h_c=10 mm) under uni-axial bending M_{xx}.

cell wall length to height ratios. The constraint along the plate boundaries are assumed to lie in between the fully clamped and the simply supported case.

A comparison of different core geometries (hexagonal and square, Figure 10) shows that hexagonal cores give higher critical dimpling loads (for t_f <0.1 mm), where square cores avoid cell wall buckling. The two aluminum-aluminum sandwiches in Figure 10 (h_c=10 mm) have the same effective core density and are loaded in x-direction. Critical modes are dimpling for thin facesheets. Cell wall buckling and facesheets yielding, respectively, is critical for thicker facesheets. Wrinkling is not critical for these stiff cores. The agreement between analytical and FE results is very good for hexagonal cores. Dimpling predictions for square cores are only approximate if the dimpling formula (Equation (24)) is used instead of the plate buckling formula (similar to Equation (27)).

The transition from dimpling to wrinkling failure (see Figure 11) is observed by using a "soft" Nomex core. If this sandwich with a hexagonal honeycomb core is loaded under bending (M_{xx}) the critical failure mode for very thin facesheets is dimpling followed by a combination of dimpling-wrinkling (see A and B in Figure 11) for moderate thick faces. The wrinkling wave length is periodic with respect to the basic cell (1×1 cell). Thicker facesheets (C and D) show a typical wrinkling pattern with increasing wave lengths, where a deviation of the analytical (homogeneous core assumption) and finite element computations (cellular core) is visible. Howeverm, at these load levels facesheet yielding is already critical.

Dimpling, wrinkling of thick and thin sandwiches as well as global buckling are observed if steel facesheets are attached to a Nomex core (Figure 12). The model consists of 35 base cells in x direction. A constant core height (h_c=25 mm) and an increasing facesheet thickness leads to dimpling for $t_f < 0.06$ mm. In the range of $0.06 < t_f <$ 0.2 mm wrinkling of thick cores is the critical mode (Figure 12, A), which is followed by thin core wrinkling. In the second case an antisymmetric wrinkling pattern (influence of opposite facesheet) is visible. Finally, a global, shear dominated buckling occurs (Figure 12, C). The analytical prediction of the wrinkling stresses is rather poor (Figure 12, A and B). In these cases one half wave (HW) is running over 0.73 (A) and 1.25 (B) honeycomb cells, which is less then the suggested value of at least 2 HW/cell for accurate analytical wrinkling predictions. However, a very good analytical prediction of global buckling is visible. The buckling length for this case is chosen as $l_k = 1.0l$, where l is the length of the finite element model in x direction.

A comparison of the wrinkling half wave length (Figure

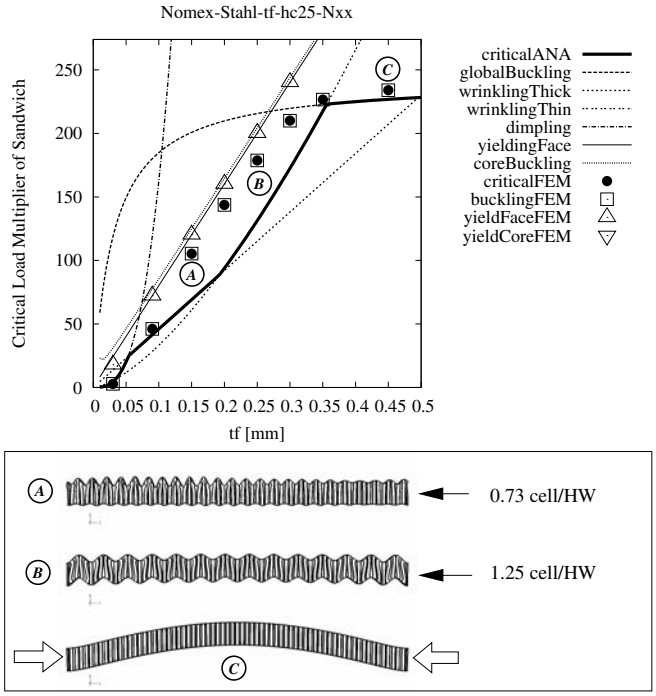

Figure 12 : Critical load multiplier λ over facesheet thickness of a steel (facesheet) - Nomex (hexagonal core) sandwich (h_c=25 mm) under uni-axial compression N_{xx}. HW/cell... half waves per unit cell.

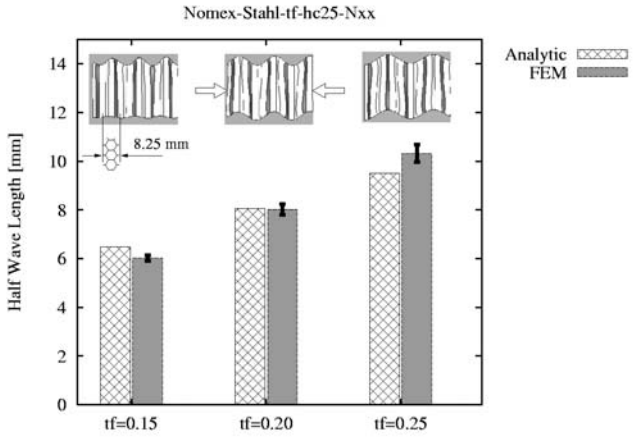

Figure 13 : Comparison of wrinkling half wave lengths for three different facesheet thicknesses (t_f=0.15, 0.20, 0.25 mm) of a steel (facesheet) - Nomex (hexagonal core) sandwich (h_c=25 mm) under uni-axial compression N_{xx}. The analytical results (crossed bars) are compared to the FEM results (solid bars, 35×1 cells). Error bars correspond to the maximum error due to the usage of a periodic FE model.

13) shows a good agreement between finite element and analytical results. The error bars assumes that the number of wrinkles within the FE model is plus/minus one half wave length. They show a very small error due to the restriction by the periodic FE model. The FE model has 35×1 cells. An increase of the cell numbers in loading direction would reduce this error. Whereas, the error in the relevant results, i.e. buckling loads, is smaller than the error in the wrinkling half wave length. For example, the difference between results obtained from a 10×1 FE model and that from the presented 35×1 model is 0.02%!

Results for local buckling loads of sandwiches under bi-axial loading are shown in Figure 14. Two core materials (aluminum and Nomex) as well as two different facesheet thicknesses are considered by the models. Thicker facesheets (t_f=0.2 mm) lead to cell wall buckling, thin facesheets (t_f=0.05 mm) to dimpling. Problems with the suggested dimpling interaction formula become obvious. For example, the rather "soft" Nomex core leads to an overestimation of the dimpling loads (Figure 14) in the range of 37.0%...99.4%. In the case of an aluminum core the obtained agreement is better (error in the range of 7.4% ...31.4%). The cell wall buckling predictions in Figure 14 by the proposed analytical model agree well with the finite element results.

4 Discussion

Dimpling can only be expected for very thin facesheets (in the considered cases approximately $t_f < 0.1$ mm). High deviations of the analytical dimpling predictions from finite element results are visible (Figure 14, A), because the dimpling formula does not take different core materials into account, i.e., the stiffness of the core material influences the accuracy of the analytical dimpling loads. A new analytical dimpling approach has to be developed. Furthermore, the interaction formula (Equation (30)) should be improved. In a first step the coefficents p might be reduced (p =1...3). A comprehensive study on this topic should be a future task.

Cell wall buckling is only found in hexagonal cores with not too thin facesheets, i.e., in the considered cases t_f >0.05 ...0.1 mm. A new model for the treatment of this instability is presented. No othre comparable approach could be found in the literature. The stiffness loss of the core due to cell wall buckling might influ-

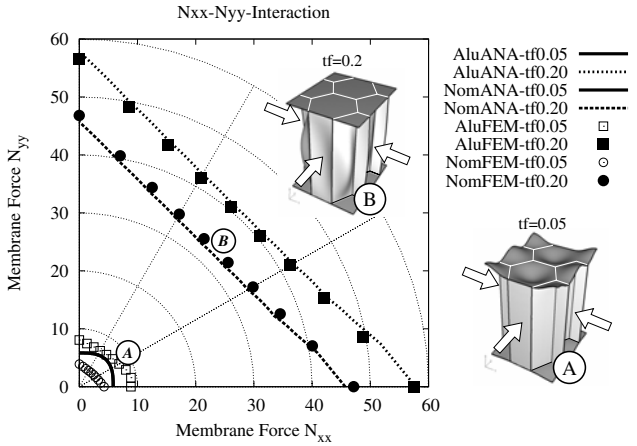

Figure 14 : Critical sandwich failure critical load multiplier λ of aluminum-aluminum sandwiches with hexagonal cores (h_c=10 mm) under bi-axial compression N_{xx}, N_{yy}. Critical analytical dimpling loads ($t_f = 0.05$) are the same for aluminum and Nomex core material.

ence the post buckling behavior of the sandwich (next visible buckling mode, e.g. wrinkling) significantly. The introduced cell wall buckling formula, which is based on CLT stress computations, is well suited for in-plane loading of the sandwich. Beside the clamping conditions, the buckling factor k is a function of core thickness as expected from the literature and lies in between a physically meaningful range. Due to the fact that the analytically computed cell wall stresses and the average finite element stresses are very similar (see Figure 8), k should not be seen as a "fitting parameter", but rather dependent on clamping conditions at the interface between core and facesheets as well as on the SW/h_c ratio.

Plastic yielding of facesheets is found to be the relevant failure mode for sandwiches under bending, where facesheet thicknesses greater than 0.1 mm (aluminum) ...0.25 mm (Nomex) exist. The analytical estimations of the stresses in the facesheets should be based on CLT in order to take multi-axial stresses into account.

Wrinkling and global shear dominated buckling is observed for very stiff (steel) facesheets and very soft (Nomex) honeycomb cores. The finite element models for these analyses are larger than the one for dimpling predictions. If at least approximately 10 ...20 wrinkling waves are realized within the FE model the error which comes from the periodicity constraint (only discrete wavelength numbers possible within the FE model) becomes negligible. The poor correlation between analytical and finite element results (Figure 12) can be explained by the assumption of a continuous core support (homogenized core material) in the analytical model. This means that one wrinkling half wave has to go over at least two honeycomb cells in order to get reliable analytical wrinkling predictions. Otherwise the core has to be considered as a discrete structure. The error which comes from the continuous core assumptions can be considerable. In the considered case (Figure 12) this error is up to 35%.

Summarizing, it can be said that for a wide range of parameters good agreements between analytical and finite elements results verify the utilized analytical formulae as well as the periodic finite element approach. Furthermore, finite element unit cell models are well suited for accurate predictions of the critical sandwich failure loads and represent a cheap reliable method (compared to experiments) to validate new analytical design formulae as well as to investigate new sandwich designs.

References

ABAQUS (2005): *Standard User's Manual, Version 6.5*. Hibbit, Karlsson & Sorensen, Inc., Pawtucket, RI, USA.

Allen, H. G. (1969): *Analysis and Design of Structural Sandwich Panels*. Pergamon Press, Oxford, UK.

Anthoine, A. (1995): Derivation of the in-plane elastic characteristics of masonry through homogenization theory. *Int. J. Sol. Struct.*, vol. 32, no. 2, pp. 137–163.

Bathe, K.-L. (1996): *Finite Element Procedures*. Prentice-Hall, Inc., NJ, USA.

Daxner, T. (2003): *Multi-Scale Modelling and Simulation of Metallic Foams*. Fortschritt-Berichte VDI Reihe 18 Nr. 285. VDI-Verlag, Düsseldorf, Germany.

Department of Defense, U. S. (1968): *Structural Sandwich Composites*. U.S. Military Handbook MIL-HNDBK-23A, Washington, DC.

Hohe, J. (2003): A direct homogenisation approach for determination of the stiffness matrix for microheterogeneous plates with application to sandwich panels. *Composites Part B*, vol. 34, pp. 615–626.

Jones, R. M. (1999): *Mechanics of Composite Materials*. Taylor and Francis Inc., Philadelphia, USA, second edition.

Lamberti, L.; Venkataraman, S.; Haftka, R.; Johnson, T. (2003): Preliminary design optimization of stiffened panels using approximate analysis models. *Int. J. Numer. Meth. Eng.*, vol. 57, pp. 1351–1380.

Léotoing, L.; Drapier, S.; Vautrin, A. (2004): Using new closed-form solutions to set up design rules and numerical investigations for global and local buckling of sandwich beams. *J. Sandwich Struct. Mat.*, vol. 6, pp. 263–289.

Ley, R.; Lin, W.; Uy, M. (1999): Facesheet wrinkling in sandwich structures. *NASA Contractor Report CR-1999-208994*.

Norris, C.; Kommers, W. (1950): Short column compressive strength of sandwhich constructions as affected by the size of cells of honeycomb core materials. *FPL Report*, vol. 1817.

Pahr, D. H. (2003): *Experimental and Numerical Investigations of Perforated FRP-Laminates*. Fortschritt-Berichte VDI Reihe 18 Nr. 284. VDI-Verlag, Düsseldorf, Germany.

Plantema, F. (1966): *Sandwich Construction*. John Wiley and Sons, Inc., New York, USA.

Suquet, P. M. (1987): *Lecture Notes in Physics - Homogenization Techniques for Composite Media*, chapter IV. Springer-Verlag, 1987.

Vonach, W. K. (2001): *A General Solution to the Wrinkling Problem of Sandwiches*. Fortschritt-Berichte VDI Reihe 18 Nr. 268. VDI-Verlag, Düsseldorf, Germany.

Vonach, W. K.; Rammerstorfer, F. G. (2001): A general approach to the wrinkling instability of sandwich plates. *Struct. Eng. Mech.*, vol. 12, pp. 363–376.

Yusuff, S. (1955): Theory of wrinkling in sandwich construction. *J. R. Aeronaut. Soc.*, vol. 59, pp. 30–36.

Zenkert, D. (1995): *An Introduction to Sandwich Construction*. EMAS Ltd., Solihull, UK.